**Astronomy
&
Astrophysics**

Abell 3560, a galaxy cluster at the edge of a major merging event

S. Bardelli[1], T. Venturi[2], E. Zucca[1], S. De Grandi[3], S. Ettori[4], and S. Molendi[5]

[1] INAF – Osservatorio Astronomico di Bologna, via Ranzani 1, 40127 Bologna, Italy
[2] Istituto di Radioastronomia del CNR, via Gobetti 101, 40129, Bologna, Italy
[3] INAF – Osservatorio Astronomico di Brera, via Bianchi 46, 23807 Merate (LC), Italy
[4] European Southern Observatory, Karl-Schwartzschild-Strasse 2, 85748 Garching, Germany
[5] Istituto di Fisica Cosmica "G. Occhialini" del CNR, via Bassini 15, 20133 Milano, Italy

Abstract. In this paper we study A3560, a rich cluster at the southern periphery of the A3558 complex, a chain of interacting clusters in the central part of the Shapley Concentration supercluster.
From a ROSAT-PSPC map we find that the X-ray surface brightness distribution of A3560 is well described by two components, an elliptical King law and a more peaked and fainter structure, which has been modeled with a Gaussian. The main component, corresponding to the cluster, is elongated with the major axis pointing toward the A3558 complex. The second component, centered on the Dumb-bell galaxy which dominates the cluster, appears significantly offset (by $\sim$0.15 h^{-1} Mpc) from the cluster X-ray centroid.
From a Beppo-SAX observation we derive the radial temperature profile, finding that the temperature is constant (at $kT \sim$ 3.7 keV) up to 8 arcmin, corresponding to 0.3 h^{-1} Mpc: for larger distances, the temperature significantly drops to $kT \sim$ 1.7 keV. We analyze also temperature maps, dividing the cluster into 4 sectors and deriving the temperature profiles in each sector: we find that the temperature drop is more sudden in the sectors which point towards the A3558 complex.
From VLA radio data, at 20 and 6 cm, we find a peculiar bright extended radio source (J1332–3308), composed of a core (centered on the northern component of the Dumb-bell galaxy), two lobes, a "filament" and a diffuse component. The morphology of the source could be interpreted either by a strong interaction of the radio source with the intracluster medium or by the model of intermittency of the central engine.

Key words. X-rays: galaxies: clusters – galaxies: clusters: general – galaxies: clusters: individual: A3560

1. Introduction

Merging has been recognized as the leading process in massive cluster formation, as a consequence of the hierarchical structure formation scenario. A large amount of numerical work has been done to study this phenomenon at all the relevant scales: among others, Ricker et al. (2001) studied in detail the physics of the plasma during the collision of two clusters under different initial conditions, while Colberg et al. (1999) analyzed the role of the cosmological environment on the merging.

From the observational point of view, the improvements of the Point Spread Function and sensitivity of the Chandra satellite led to the detailed description of the shocks (Markevitch et al. 2002) and the discovery of the so-called "cold fronts" (Vikhlinin et al. 2001), which are direct consequences of merging at an advanced state.

Little work has been done on the global, multiscale description of this phenomenon. To this end, we are carrying on a long term project aimed at studying the merging in the particularly rich environment of the central part of the Shapley Concentration supercluster. In this region, three "cluster complexes" are found (Zucca et al. 1993), i.e. structures of $\sim$7 h^{-1} Mpc (hereafter $h = H_0/100$) which represent major cluster mergings at various evolutionary stages.

The most massive structure, the A3558 complex (Fig. 1), is probably a collision seen after the first core-core encounter (Bardelli et al. 1998b). The whole complex, formed by a chain of three ACO clusters and two poor groups, is embedded in a hot gas filament (Bardelli et al. 1996; Kull & Böhringer 1999) and in a common envelope of galaxies (Bardelli et al. 1994, 1998a). The estimated mass ranges between 10^{15} and 10^{16} $M_\odot$ (Bardelli et al. 2000; Ettori et al. 1997; Reisenegger et al. 2000).

The entire structure presents a large number of substructures, some of which have an X-ray counterpart as diffuse emission (Bardelli et al. 2002). Moreover, the merging seems to lead to a lack of radio sources with respect to "normal" clusters (Venturi et al. 2000). The presence of a halo radio source, of a minihalo and a relic radio source (Venturi et al., in preparation) is further evidence of "stormy weather".
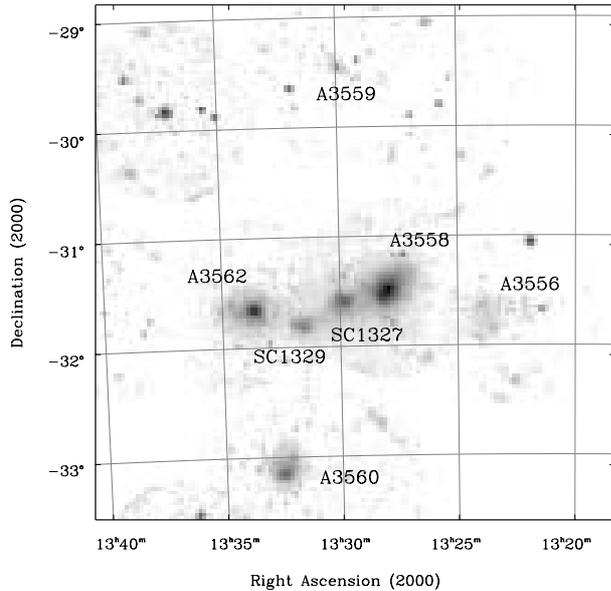
Fig. 1. Large scale view of the center of the Shapley Concentration centered on the A3558 complex. This image is a mosaic of all the pointed ROSAT-PSPC frames available in this region (see Ettori et al. 1997). Note the position of the cluster A3560 (on the bottom).

In this paper we concentrate on the cluster A3560, a rich cluster at the southern periphery of the A3558 complex. In Fig. 1 a mosaic of the available ROSAT-PSPC frames is shown and gives the large-scale distribution of the clusters in this region. The two groups labelled SC 1327 and SC 1329 are SC 1327 − 312 and SC 1329 − 313.

The distance of A3560 from the nearest X-ray clump of the A3558 complex (corresponding to SC 1329 − 313) is $\sim$3 h^{-1} Mpc. Given the proximity of such a large mass concentration, the high predicted infall velocity ($\sim$2000 km s^{-1}, Reisenegger et al. 2000) and the existence of the underlying overdensity of the supercluster (see Bardelli et al. 2000), a certain degree of disturbance can be expected for A3560.

The plan of the paper is the following. In Sect. 2 we describe the general properties of A3560 and in Sect. 3 we perform the spatial analysis of the ROSAT-PSPC map. In Sect. 4 we analyze our new Beppo-SAX observations on this cluster, obtaining temperature profiles and maps, while in Sect. 5 we present the properties of the central radio source of A3560. Finally in Sect. 6 we discuss and summarize the results.

2. The cluster A3560

Abell 3560 is a cluster of richness class 3 and Bautz-Morgan class I; the center has coordinates $\alpha_{2000} = 13^h32^m22^s$, $\delta_{2000} = -33°05'24''$. Note that the position reported by Abell et al. (1989), i.e. $\alpha_{2000} = 13^h31^m50^s$ and $\delta_{2000} = -33°13.4'$, corresponds neither to an optical overdensity nor to a diffuse X-ray emission. Probably, there was a mistake in reporting the position, considering that nearby this position a bright galaxy is located (NGC 5193): given its redshift ($z \sim 0.012$), this galaxy is not associated with the cluster. More details about this discrepancy can be found in Willmer et al. (1999) and references therein.
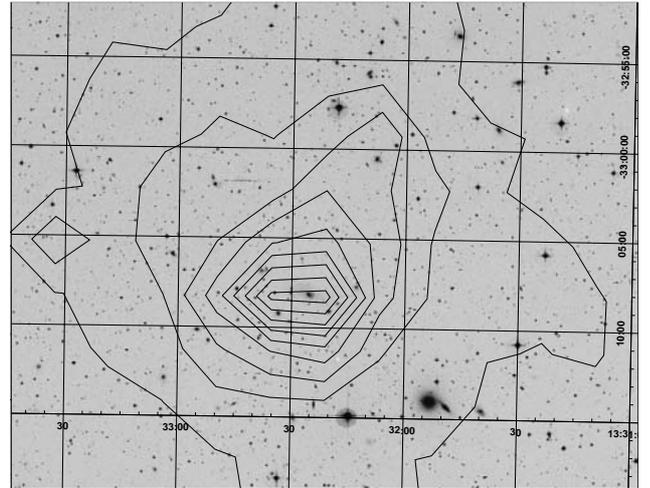

Fig. 2. X-ray isophotes, from a ROSAT-PSPC observation pointed on A3560, superimposed on the optical image from the Digital Sky Survey. The bright elliptical galaxy (with a nearby edge-on spiral) in the lower right corner is NGC 5193. See the text for further details about the isophotes.

On the basis of 32 redshifts, Willmer et al. (1999) estimated $\langle v \rangle = 14470 \pm 123$ km s^{-1} and $\sigma = 614 \pm 68$ km s^{-1} and detected a marginal significance of substructure by applying the Lee 2-3D statistics.

This cluster is dominated by a Dumb-bell galaxy: Willmer et al. (1999) reported the velocities of the two components, consistent each other within the errors and at rest with the cluster velocity centroid.

At the redshift of the cluster ($z = 0.048$), assuming $q_0 = 0.5$, 1 arcmin corresponds to $\sim$38.56 h^{-1} kpc.

3. ROSAT spatial analysis

ROSAT-PSPC data for A3560 have been taken from the public *HEASARC* archive, and are part of the $\sim$6000 s observation referenced as RP800381A02. In Fig. 2 we present the X-ray isophotes superimposed on the optical image from the Digital Sky Survey: the contours refer to the inner 20′ of the ROSAT-PSPC data, where the vignetting is small. The data have been smoothed with a Gaussian of 10 pixel *FWHM* (1 pixel = 15 arcsec) and the linear step between contours is 0.30, with the lowest isophote corresponding to 0.282 cts pix^{-1} (well above the background value, see below). Already at a first look at the image, it is clear that the cluster is formed by two components with offset centers: one symmetric, circular component and one elongated, more extended contribution.

For this reason, following Bardelli et al. (1996), we fitted the surface brightness distribution using an elliptical King law and a Gaussian of the form

$$P(x,y) = I_o \left[1 + \left(\frac{x'}{R_1} \right)^2 + \left(\frac{y'}{R_2} \right)^2 \right]^{-3\beta+0.5}$$

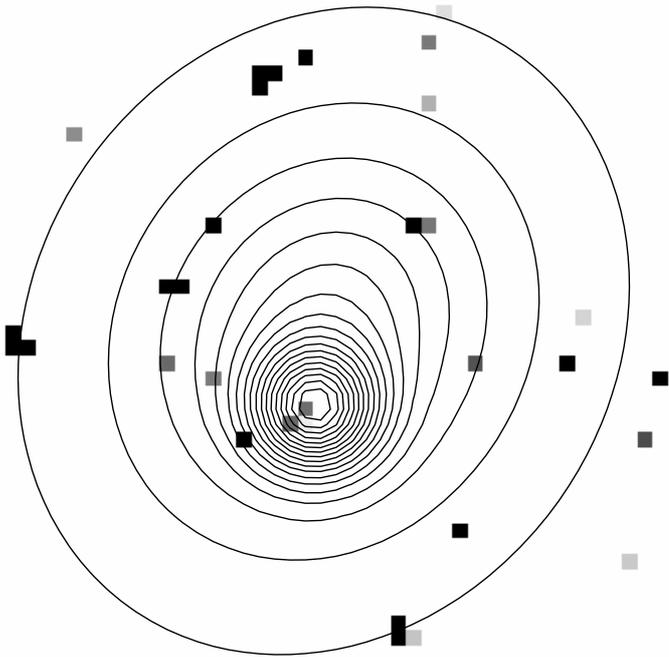$$+ I_g \exp \left[\frac{(x - x_g)^2 + (y - y_g)^2}{2\sigma^2} \right] + bck \qquad (1)$$

Fig. 3. Model isodensity contours superimposed to a χ^2 map of the difference model-data. The pixels have a 3×3 rebinning with respect to the original frame. Visible points correspond to $\chi^2 > 6$ and have been clipped from the fit.

where

$$x' = (x - x_k) \cos \theta + (y - y_k) \sin \theta$$
$$y' = -(x - x_k) \sin \theta + (y - y_k) \cos \theta$$

in order to take into account the position angle θ of the cluster. The variables to be estimated are the two normalizations I_o and I_g, the positions (x_k, y_k) and (x_g, y_g) of the centers of the cluster and of the Gaussian respectively, the position angle of the cluster (θ), its core radii (R_1 and R_2), the exponent of the King law (β), the width of the Gaussian (σ). The background (bck) has been estimated by averaging the count-rates in 9 areas in the external parts of the map, and resulted to be 0.0781 ± 0.0029 cts pix^{-1}.

The fit has been performed by minimizing the χ^2 variable between the model and the data, after having rebinned (3×3 pixels) the original image. A number of strongly ($\chi^2 > 6$) deviant pixels, which likely correspond to real sources, have been eliminated from the fit procedure. The results of the fit, done in the [0.5–2.0] keV band, are reported in Table 1.

In Fig. 3 we show the model isodensity contours superimposed to a χ^2 map of the difference model-data. The pixels have a 3×3 rebinning with respect to the original frame.

The centers of the two components resulted to be separated by 15.39 pixels (3.8 arcmin), corresponding to 0.15 h^{-1} Mpc. In order to verify if the peaked component is really a Gaussian, we subtracted the King model from the data map and analyzed the residuals separately with various image fitting packages. In all cases the Gaussian model was compatible with the data and the dispersion parameter consistent with our ones.

The position angle of the King model is tilted 32 degrees westward with respect to the North direction: note that this

value is close to the direction toward A3558 (~30 degrees), which is ~4.6 h^{-1} Mpc away from A3560 and is thought to be the barycenter of the A3558 cluster complex.

4. Beppo-SAX spectral analysis

4.1. Observations and data reduction

The cluster A3560 was observed by the Beppo-SAX satellite (Boella et al. 1997a) in the period 1–3 July 2000, with a total exposure time of 65.5 ksec.

Here we discuss the data from two of the instruments onboard Beppo-SAX: the Medium-Energy Concentrator Spectrometer (MECS) and the Low-Energy Concentrator Spectrometer (LECS). The MECS (Boella et al. 1997b) is composed of two units, working in the [1–10] keV energy range. At 6 keV, the energy resolution is ~8% and the angular resolution is ~0.7′ (*FWHM*). The LECS (Parmar et al. 1997), consists of an imaging X-ray detector, working in the [0.1–9] keV energy range, with 20% spectral resolution and 0.8′ (*FWHM*) angular resolution (both computed at 1 keV). Standard reduction procedures and screening criteria have been adopted to produce linearized and equalized event files. The MECS (LECS) data preparation and linearization was performed using the SAXDAS (SAXLEDAS) package under FTOOLS environment.

We have taken into account the PSF-induced spectral distortions (D'Acri et al. 1998) in the MECS analysis using effective area files produced with the *effarea* program. All MECS and LECS spectra have been background subtracted using spectra extracted from blank sky event files in the same region of the detector as the source (see Fiore et al. 1999). A detailed explanation of the MECS analysis is given in De Grandi & Molendi (2001).

As done in Ettori et al. (2000), for the LECS we have used two redistribution matrices and ancillary response files, the first computed for an on-axis pointlike source and the second for a source with a flat brightness profile. The temperatures and abundances we derive in the two cases do not differ significantly, as the telescope vignetting in the [0.1–4.0] keV energy range is not strongly dependent upon energy. All spectral fits have been performed using XSPEC Ver. 10.00, fitting the data with a *mekal* (Mewe et al. 1995; Kaastra 1992) model, absorbed for the nominal Galactic hydrogen column density (*wabs* model). The hydrogen column has been fixed to the value of 4.1×10^{20} cm^{-2} (Dickey & Lockman 1990).

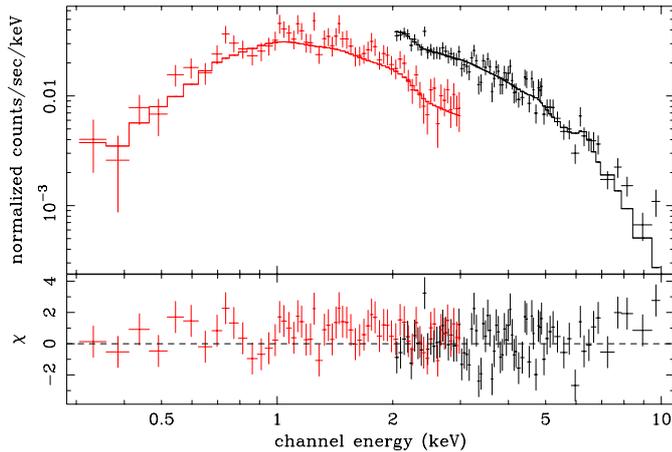### 4.2. Global temperature

We fitted the spectrum of A3560 within 8 arcmin (corresponding to ~0.3 h^{-1} Mpc). First we estimated the temperature and abundance from the two combined MECS instruments, in the [2–10] keV range. We found $kT = 3.80^{+0.37}_{-0.32}$ keV and an abundance $0.10^{+0.10}_{-0.10}$, where the errors are at the 90% significance level. The reduced χ^2 is 1.44 with 109 degrees of freedom.

The temperature and abundance determination for the LECS in the range [0.3–3] keV gives $kT = 3.34^{+0.99}_{-0.66}$ keV and abundance $0.33^{+0.73}_{-0.33}$, with 1.08 of reduced χ^2 and 251 degrees of freedom.

Table 1. Results of the bi-dimensional fit (errors are at 1σ level).

Component	Normalization	core radii/σ	β	θ
King	0.93 ± 0.05 cts pix^{-1}	$33.75 \pm 1.63 - 28.86 \pm 1.44$ pix	0.525 ± 0.022	$32° \pm 5°$
	3.20×10^{-7} erg str^{-1} cm^{-2} s^{-1}	$0.325 - 0.278$ h^{-1} Mpc		
Gaussian	1.69 ± 0.38 cts pix^{-1}	8.08 ± 0.42 pix		
	6.07×10^{-7} erg str^{-1} cm^{-2} s^{-1}	0.08 h^{-1} Mpc		

Fig. 4. Spectrum and fit of the MECS+LECS data within 8 arcmin from the center of A3560.

Fig. 5. Temperature radial profile of A3560. The vertical bars correspond to 68% errors, while the horizontal bars represent the bins used to extract the counts. The dotted line corresponds to the global fit, derived within 8 arcmin.

Given the fact that these estimates are consistent with each other, in order to enhance the statistics we fitted the combined LECS+MECS data. First, we ran the fit by estimating also the relative normalization between the two instruments: having checked that this number is consistent (within one sigma) with the standard value of 0.5, we fixed it at 0.5. The results (see Fig. 4) are $kT = 3.69^{+0.24}_{-0.22}$ keV and abundance $0.13^{+0.10}_{-0.09}$ with a reduced χ^2 of 1.19 and 363 degrees of freedom.

The temperature is in agreement with the value of 3.4 keV estimated by Ebeling et al. (1996) on the basis of the $L_X - T$ relation.
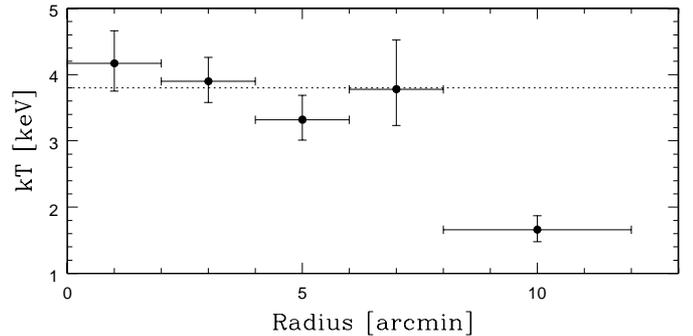
Following the $\sigma - T$ relation of Lubin & Bahcall (1993) $[\sigma = 332(kT)^{0.6}$ km s$^{-1}]$, the determined temperature implies a velocity dispersion of 727^{+17}_{-17} km s^{-1} (one sigma errors), which is consistent at 1.6 sigma with the value estimated by Willmer et al. (1999).

With the estimated temperature, the total luminosity within 16 arcmin is $L_{[2-10]\ keV} = 3.6 \times 10^{43}$ h^{-2} erg s^{-1} corresponding to a bolometric luminosity of $L_X = 7.1 \times 10^{43}$ h^{-2} erg s^{-1} well consistent with the PSPC-ROSAT value of $L_X = 6.9 \times 10^{43}$ h^{-2} erg s^{-1} estimated by David et al. (1999).

4.3. Temperature profiles and maps

In analysing temperature profiles and maps we used only the MECS data, for which the correction for the PSF-induced spectral distortions is available.

The cluster emission has been divided into concentric annuli, centered on the X-ray emission peak: out to 8 arcmin the annuli are $2'$ wide, beyond this radius the annuli are $4'$ wide. To all spectra accumulated from these annular regions, we have applied the model described in Sect. 4.1 to derive temperature and metal abundances. The fitting procedure stops at the last annulus where the source counts are more than 30% of the total (i.e. source plus background) counts (see the discussion in De Grandi & Molendi 2002).

In Fig. 5 we report the temperature profile of A3560 in annuli around the cluster center. The vertical bars correspond to the 68% errors and the horizontal bars represent the bins used to extract the counts. The dotted line corresponds to the value obtained from the global fit.

Regarding the abundance, the values derived in the first three bins are consistent with the global determination, while the fit was unconstrained for the last two points. Therefore for radii larger than 6 arcmin the plotted temperatures were derived fixing the abundance to the global value.

The profiles are in agreement with those obtained by Bonamente et al. (2001) using ROSAT-PSPC data. In particular, it is encouraging that at large distances from the center ($\sim$10 arcmin), they show the same low temperature: given the fact that this is an independent estimate, the result is not an artifact of the MECS or of our background subtraction procedure. The spectral fit of the data in the last annulus is shown in Fig. 6: the temperature is $1.65^{+0.37}_{-0.30}$ keV and the reduced χ^2 is 1.03 with 62 degrees of freedom. We note however that the robustness of the MECS temperature estimate at such distances was already demonstrated by Bardelli et al. (2002): with the use of two different overlapping exposures, we measured the temperature of the same point once with the inner part of the MECS and once with the external part, finding the same result.
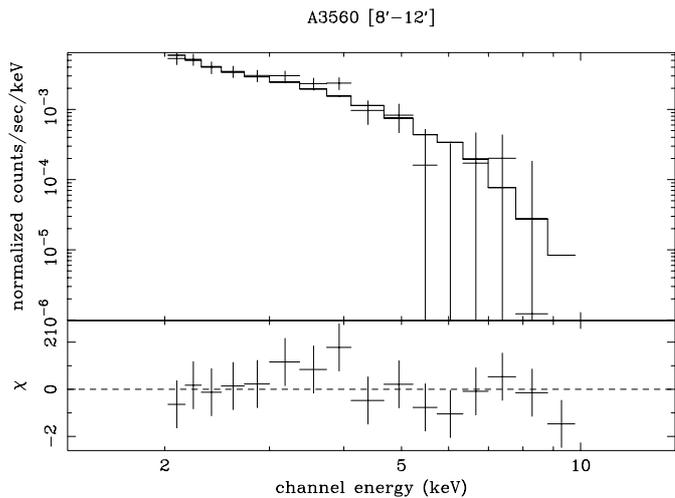
Fig. 6. Spectrum, fit and residuals of the MECS data in the 8–12 arcmin annulus.
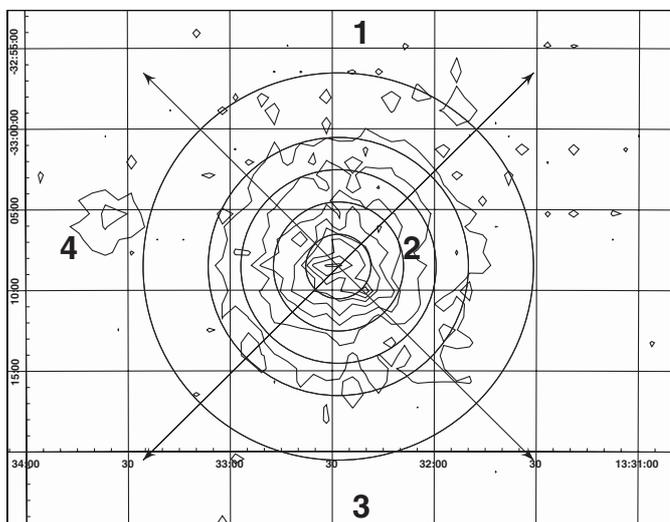

Fig. 7. Beppo-SAX MECS image of A3560. The image has been smoothed with a Gaussian of 6 pixels *FWHM*, corresponding to 0.8 arcmin. The concentric circles correspond to the bins of the radial profile, while the quadrants correspond to the sectors used for the temperature map analysis. In this case, the third and fourth shells have been used as a single radial bin.

The first point of Bonamente et al. (2001), corresponding to our first two radial bins, although at lower temperature (2.2 keV), is still consistent with our determinations. However, due to the different energy range, the PSPC is more sensitive to lower temperature than the MECS and therefore we cannot rule out the existence of a multiphase medium.

In order to explore if there is an asymmetry of the temperature distribution due to the interaction of the intracluster medium with possible material of the A3558 complex, we divided the cluster map in four sectors as shown in Fig. 7. Sector 1 is North of the image and the numbers increase clockwise. In order to increase the statistics, we used the third and fourth shells as a single radial bin. In Fig. 8 the temperature profiles in the four sectors are presented. In all the quadrants the last point is consistent to be at the same low temperature,
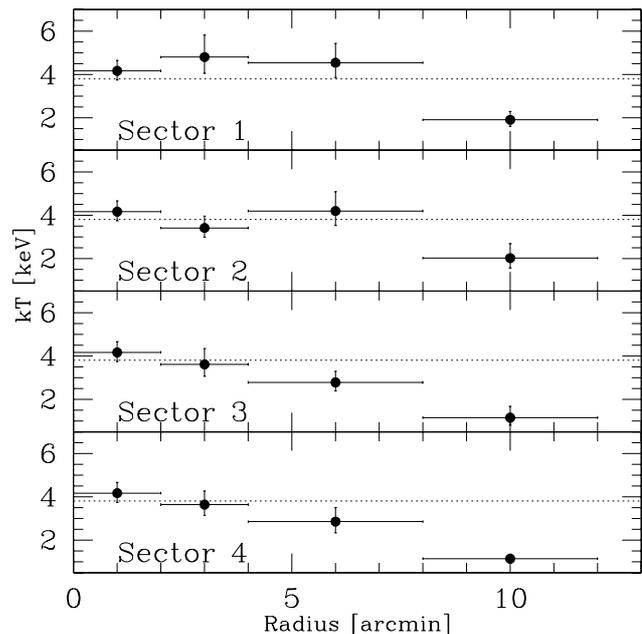

Fig. 8. Temperature map of A3560. The vertical bars correspond to 68% errors, while the horizontal bars represent the bins used to extract the counts. Dotted lines are drawn in correspondence of the global fit temperature.

but the temperature drop is more sudden in sectors 1 and 2, while it is smoother in the other sectors. Indeed, the temperature derived in the $4'-8'$ annulus from the combined fit of sectors $1 + 2$ is $4.34^{+1.10}_{-0.75}$ keV, while for sectors $3 + 4$ it is $2.80^{+0.71}_{-0.47}$ keV: therefore the values are different at $\sim 2.5\sigma$ confidence level.

Considering the region where the cluster is isothermal, at the global temperature of $kT = 3.69$ keV, the derived total mass is $M(< 0.3\ h^{-1}\ \mathrm{Mpc}) = (3.08 \pm 0.19) \times 10^{13}\ h^{-1}\ M_\odot$. If we extrapolate this mass up to a radius of $1\ h^{-1}$ Mpc, we find $M(< 1\ h^{-1}\ \mathrm{Mpc}) = (1.89 \pm 0.12) \times 10^{14}\ h^{-1}\ M_\odot$, consistent within the errors with the value of $1.64^{+0.93}_{-0.77} \times 10^{14} M_\odot$ given by Willmer et al. (1999), based on optical data within 30 arcmin (corresponding to $\sim 1.16\ h^{-1}$ Mpc). However, given the fact that this cluster presents a temperature gradient, this extrapolation cannot be considered reliable. We tried to model the gradient in the gas temperature with a polytropic profile (Ettori 2000), finding an index $\gamma \geq 2$: this indicates that the intracluster medium is unstable to convective mixing, with turbulent motions that relax to an homogeneous gas after several sound crossing times $[t_s(10\ \mathrm{arcmin}) \approx 1.5 \times 10^9\ h^{-1}\ \mathrm{yr} \approx 0.25\ t_{\mathrm{age\ Universe}}]$. This fact questions the validity of the hydrostatic equilibrium hypothesis for regions at distances $> 0.3\ h^{-1}$ Mpc from the cluster center.

The situation of the Gaussian component is also complex, because of the lack of temperature determination. The MECS and LECS instruments do not have enough spatial resolution to separate the spectra of the Gaussian component from the King model; moreover, the luminosity of the Gaussian component is only $\sim 2\%$ of the total luminosity. The best direct measurement can be considered the central point of Bonamente et al. (2001) at $kT = 2.2^{+1.5}_{-0.6}$ keV, obtained from a ROSAT-PSPC map. Note that, although this spike is cooler than the cluster, there is no cooling flow: in fact, we derived a cooling time of 3.9×10^{13} yr.
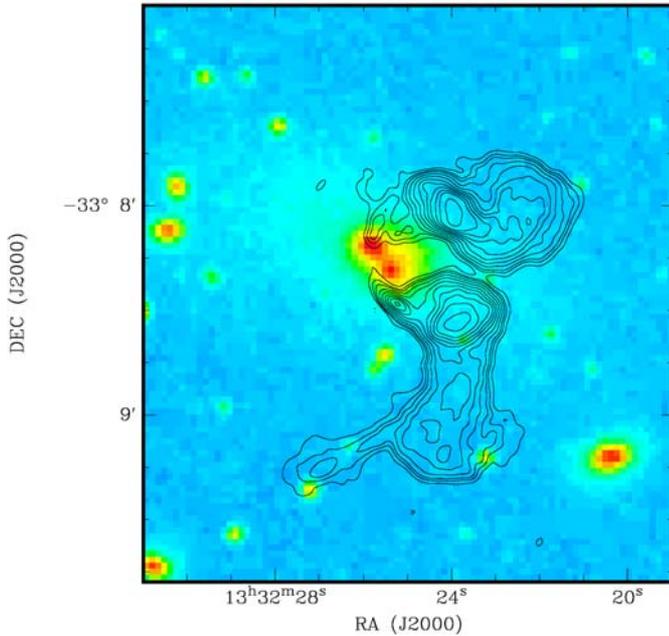
Fig. 9. Radio isocontours at a wavelenght of 20 cm superimposed to the optical image taken from the Digital Sky Survey (DSS2). The resolution is 4.2×3.7 arcsec with a position angle of $61°$. The map noise is 0.14 mJy/beam and the first contour correspond to 0.45 mJy/beam. The other nth contours are spaced by a factor 2^n.

Fig. 10. Radio isocontours at a wavelenght of 6 cm. The resolution is 2.1×1.2 arcsec with a position angle of $5°$. The map noise is $46\,\mu$Jy/beam and the first contour corresponds to 0.15 mJy/beam. The other nth contours are spaced by a factor 2^n.

In order to have an independent temperature estimate, we followed a more indirect way: we calculated the densities of the King and of the Gaussian models at the center of the latter and imposed pressure equilibrium. In this case $n_e^K kT^K = n_e^G kT^G$, where the indexes "K" and "G" refer to the two models. Given the fact that n_e^G depends on kT^G, we solve the equation iteratively, finding $kT^G = 1.12$ keV.

The pressure found at the center of the Gaussian results in $P = 3.73 \times 10^{-12}\,h^{0.5}$ dyn cm^{-2}. However, in the case where the Gaussian component has a temperature of $kT = 2$ keV, the pressure is $P = 5.90 \times 10^{-12}\,h^{0.5}$ dyn cm^{-2}: in this case the pressure balance with the cluster is reached at a distance from the center of the order of $\sim 0.08\,h^{-1}$ Mpc, corresponding to 1σ of the Gaussian. These estimates can only give an idea of the pressure inside the density spike in order to study the central radio source (see Sect. 5), but we have to take in mind the possibility that this entity is not at all at pressure equilibrium.

5. The radio galaxy J1332–3308

At radio wavelengths A3560 is dominated by the extended radio galaxy J1332–3308, associated with the Dumb-bell galaxy cited in Sect. 2. This source is located approximately at the center of the peaked component of the hot gas distribution (see Sect. 3). No other radio sources in the A3560 field are associated with cluster galaxies.

This radio galaxy was observed over a wide range of radio frequencies with the Very Large Array (VLA, New Mexico, USA) and with the Australia Telescope Compact Array (ATCA, Narrabri, Australia) as part of a larger project addressing extended radio galaxies in the central region of
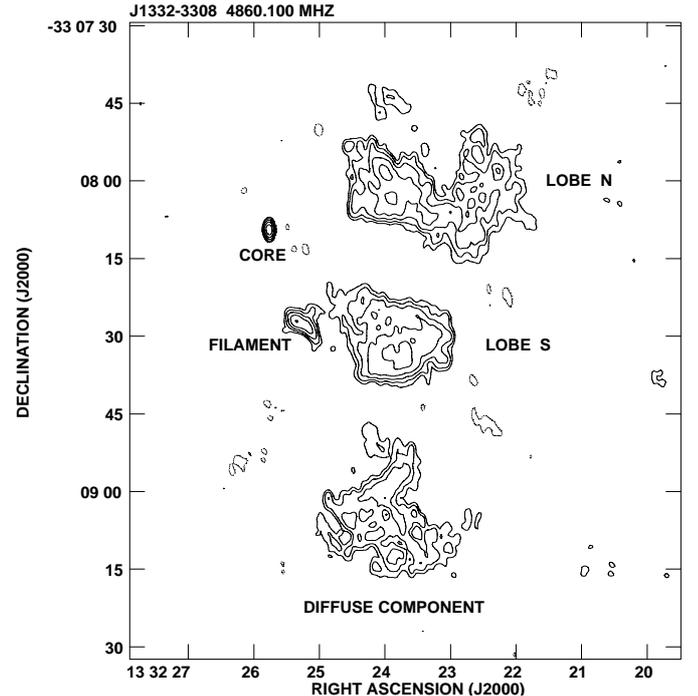
the Shapley Concentration (Venturi et al. in preparation). In this section we will present only those radio properties of this source relevant to the astrophysical problems dealt with in the present paper.

In Fig. 9 we show the 1.4 GHz VLA image of the radio galaxy overlaid on the DSS–2 optical image. As can be seen, J1332–3308 is a complex radio source, as is often found at the centre of galaxy clusters, with a total power of $\log P(\text{WHz}^{-1}) = 24.41$ at 1.4 GHz. This value can be considered the transition power between FRI and FRII radio galaxies (Fanaroff & Riley 1974), and among the largest values found for radio galaxies located at the centre of rich clusters (Burns 1990; Ball et al. 1993; Gregorini et al. 1994). The origin of the radio emission is likely to be associated with the north-eastern component of the Dumb-bell galaxy.

The higher resolution image at the wavelength of 6 cm (Fig. 10) suggests that the overall morphology of the radio galaxy includes five different components: the nucleus of the radio emission, associated with the north-eastern optical nucleus of the optical counterpart, two "fat" and extended lobes, labelled lobe N and lobe S, a small filament of radio emission located South of the radio core (pointing southwards), and a diffuse extended emission South of the lobe S. The connection between these components is unclear, and a detailed discussion will be carried out in Venturi et al. (in preparation). One possibility is that all components are coeval, and that the complex morphology is the result of cluster weather, i.e. interaction with the surrounding intracluster gaseous medium (Burns 1998), possibly combined with orientation effects of the radio emission. One alternative possibility is that J1332–3308

Table 2. Physical parameters of J1332–3308.

Component	$\alpha_{1.4}^{8.6}$	B_{eq} μG	P_{eq} (10^{-12}) $h^{4/7}$ dyn cm^2
Core	0.47	32.6	131.1
Lobe N	0.94	5.4	3.6
Lobe S	0.75	5.9	4.4
Filament	0.81	14.7	26.8
Diffuse	0.74	4.2	2.2

consists of one "active" part, the nucleus and the two extended lobes N and S, and of one "relic" emission, the filament and the diffuse southern structure.

We estimated the equipartition parameters for this source, using all the interferometric images available from 1.4 GHz to 8.6 GHz. They are summarised in Table 2. The entries in the table are: the component as described above (Col. 1); the spectral index in the range 1.4 GHz–8.6 GHz, to be read in the sense $S \propto \nu^{-\alpha}$ (Col. 2); the equipartition magnetic field (Col. 3); the internal pressure at equipartion (Col. 4). We note that the equipartition parameters were computed taking into account cylindric geometry, a filling factor $\Phi = 1$ and a ratio between protons and electrons $K = 1$.

The equipartition parameters in the extended components (lobes and filament) are those expected for the lobes and tails of extended sources in clusters of galaxies (Feretti et al. 1992). Overall, J1332–3308 is in pressure equilibrium with the external medium (see Sect. 3).

6. Conclusions

In this paper we studied A3560, a rich cluster (richness class 3) at the southern periphery of the A3558 complex, a chain of interacting clusters in the central part of the Shapley Concentration supercluster.

From the ROSAT-PSPC map we found that the X-ray surface brightness distribution of A3560 is well described by two components, an elliptical King law and a more peaked and fainter structure, which has been modeled with a Gaussian. The main component, corresponding to the cluster, is elongated with the major axis pointing toward the A3558 complex. The second component, centered on the Dumb-bell galaxy which dominates the cluster, appears significantly offset (by ~0.15 h^{-1} Mpc) from the cluster X-ray centroid. However, the contribution of this component to the global luminosity is only ~2%.

From the Beppo-SAX observation we derived the radial temperature profile, finding that the temperature is constant (at $kT \sim 3.7$ keV) up to 8 arcmin, corresponding to 0.3 h^{-1} Mpc: for larger distances, the temperature significantly drops to $kT \sim 1.7$ keV. This drop questions the validity of the hydrostatic equilibrium hypothesis for regions at distances >0.3 h^{-1} Mpc from the cluster center. We also analyzed temperature maps, dividing the cluster into 4 sectors and deriving the temperature profiles in each sector: we found that the temperature drop is significantly more sudden in sectors 1

and 2 (which point towards the A3558 complex), while it is smoother in the other sectors.

From the VLA radio data, at 20 and 6 cm, we found a peculiar bright extended radio source (J1332–3308), composed of a core (centered on the northern component of the Dumb-bell galaxy), two lobes, a "filament" and a diffuse component. The filament is not aligned with any of the two lobes and seems to point towards the diffuse component.

At a first look this source seems a Wide Angle Tail source, but the filament and the diffuse component do not fit this scenario. We suggest two possible interpretations of this:

i) all components are related to the same nuclear activity: in this case the filament and the diffuse emission are due to a strong interaction of the radio source with the intracluster medium. This interaction could originate from the offset position of the peaked X-ray component hosting the radio source with respect to the overall cluster (see Fig. 3). This offset can suggest a motion of the peaked component roughly along the major axis of the cluster: the consequent ram pressure can be responsible for the peculiarity of the radio source.

ii) The components are the result of an intermittency of the nuclear engine, following the model invoked for 3C 338 by Burns et al. (1983): in this case the filament and the diffuse component are the remnants of a previous activity of the radio source, while the core and the lobes are the result of the present activity of the same source. As in case i), also in this scenario a motion of the radio core in the North-South direction is required. The only difference with respect to 3C 338 is that in our case all components have flatter spectral indexes, indicating that J1332–3308 is younger.

Further investigations are needed to discriminate between these models: in particular, the interaction between the radio source and the cluster diffuse emission is a typical topic where the high resolution power of the Chandra satellite will be decisive.

As a general conclusion, the elongation in the direction of the A3558 complex, the offset of the peaked component with respect to the centroid of the cluster and its motion (suggested by the radio data) and the sudden drop in the temperature profile seem to indicate that A3560 is a dynamically disturbed cluster.

References

Abell, G. O., Corwin, H. G. Jr., & Olowin, R. P. 1989, ApJS, 70, 1
Ball, R., Burns, J. O., & Locken, C. 1993, AJ, 105, 53
Bardelli, S., Zucca, E., Vettolani, G., et al. 1994, MNRAS, 267, 665
Bardelli, S., Zucca, E., Malizia, A., et al. 1996, A&A, 305, 435
Bardelli, S., Zucca, E., Zamorani, G., Vettolani, G., & Scaramella, R. 1998a, MNRAS, 296, 599
Bardelli, S., Pisani, A., Ramella, M., Zucca, E., & Zamorani, G. 1998b, MNRAS, 300, 589

Bardelli, S., Zucca, E., Zamorani, G., Moscardini, L., & Scaramella, R. 2000, MNRAS, 312, 540

Bardelli, S., De Grandi, S., Ettori, S., et al. 2002, A&A, 382, 17

Boella, G., Butler, R. C., Perola, G. C., et al. 1997a, A&AS, 122, 299

Boella, G., Chiappetti, L., Conti, G., et al. 1997b, A&AS, 122, 327

Bonamente, M., Lieu, R., Nevalainen, J., & Kaastra, J. S. 2001, ApJ, 547, L7

Burns, J. O., Schwendeman, E., & White, R. E. 1983, ApJ, 271, 575

Burns, J. O. 1990, AJ, 99, 14

Burns, J. O. 1998, Science, 280, 400

Colberg, J. M., White, S. D. M., Jenkins, A., & Pearce, F. R. 1999, MNRAS, 308, 593

D'Acri, F., De Grandi, S., & Molendi, S. 1998, Nuclear Phys., 69/(1-3), 581

David, L. P., Forman, W., & Jones, C. 1999, ApJ, 519, 533

De Grandi, S., & Molendi, S. 2001, ApJ, 551, 153

De Grandi, S., & Molendi, S. 2002, ApJ, 567, 163

Dickey, J. M., & Lockman, F. J. 1990, ARA&A, 28, 215

Ebeling, H., Voges, W., Bohringer, H., et al. 1996, MNRAS, 281, 799

Ettori, S., Fabian, A. C., & White, D. A. 1997, MNRAS, 289, 787

Ettori, S. 2000, MNRAS, 311, 313

Ettori, S., Bardelli, S., De Grandi, S., et al. 2000, MNRAS, 318, 239

Fanaroff, B. L., & Riley, J. M. 1974, MNRAS, 167, 31

Feretti, L., Perola, G. C., & Fanti, R. 1992, A&A, 265, 9

Fiore, F., Guainazzi, M., & Grandi, P. 1999, Cookbook for Beppo-SAX NFI Spectral Analysis

Gregorini, L., de Ruiter, H. R., Parma, P., et al. 1994, A&AS, 106, 1

Kaastra, J. S. 1992, An X-Ray Spectral Code for Optically Thin Plasma, Internal SRON-Leiden report, updated version 2.0

Kull, A., & Böhringer, H. 1999, A&A, 341, 23

Lubin, L. M., & Bahcall, N. A. 1993, ApJ, 415, L17

Markevitch, M., Gonzales, A. H., David, L., et al. 2002, ApJ, 567, L27

Mewe, R., Kaastra, J., & Liedhal, K. 1995, Legacy, 6, 16

Parmar, A. N., Martin, D. D. E., Bavdaz, M., et al. 1997, A&AS, 122, 309

Reisenegger, A., Quintana, H., Carrasco, E. R., & Maze, J. 2000, ApJ, 120, 523

Ricker, P. M., & Sarazin, C. L. 2001, ApJ, 561, 621

Venturi, T., Bardelli, S., Morganti, R., & Hunstead, R. W. 2000, MNRAS, 314, 594

Vikhlinin, A., Markevitch, & M., Murray, S. S. 2001, ApJ, 551,160

Willmer, C. N., Maia, M. A. G., Mendes, S. O., et al. 1999, AJ, 118, 1131

Zucca, E., Zamorani, G., Scaramella, R., & Vettolani, G. 1993, ApJ, 407, 470